

3D QSAR and pharmacophore studies on inhibitors of insulin like growth factor 1 receptor (IGF-1R) and insulin receptor (IR) as potential anti-cancer agents



Mustafa Kamal Pasha^{a,b,*}, Ishrat Jabeen^a, Sandhya Samarasinghe^b

^a Research Center for Modeling and Simulation, National University of Sciences and Technology, Islamabad, Pakistan

^b Complex Systems, Big Data and Informatics Initiative (CSBII), Lincoln University, New Zealand

ARTICLE INFO

Keywords:

IGF1R
IR
Dual inhibitors
Tyrosine kinase domain
Small molecule inhibitors
GRIND
QSAR
Pharmacophore

ABSTRACT

Insulin like growth factor receptor (IGF-1R) and Insulin receptor (IR) are widely accepted to play a prominent role in cancer drug discovery due to their well-established involvement in various stages of tumorigenesis. Previously, neutralization of IGF-1R via monoclonal antibodies was in focus, which failed because of compensatory activation of IR-A upon inhibition of IGF-1R. Recent studies have demonstrated high homology between IGF-1R and IR particularly in tyrosine kinase domain and targeting both receptors have produced efficient therapeutic approaches such as inhibition of cancer cell cycle proliferation. Herein, we have made an attempt to analyze the unique data set from different chemical classes, containing potent ATP competitors against tyrosine kinase domain. We performed the 2D, 3D quantitative structure–activity relationship (QSAR) studies on inhibitors of these receptors to predict useful pharmacophoric features. We have optimized virtual screening of structurally diverse data set of dual inhibitors of IGF-1R and IR. Based on QSAR studies, we predict potential novel clinical candidates with a demonstrated absorption, distribution, metabolism, elimination, and toxicology (ADMETox) track. We also demonstrated comprehensive analysis of co–crystal complexes along with their inhibitors and built 3D- GRIND Independent Descriptors (GRIND) model to obtain insightful features such as H-bond donors and acceptors, overall topology and Vander Waal volume (vdw_vol) which are found to be responsible for dual inhibition of receptors. These findings lead to further description that Tirofiban, Praxolol, Edoxaban, Novobiocin have potential to perform dual inhibition of both targets.

1. Introduction

The Insulin like growth factor receptor-1 (IGF-1R) is a transmembrane receptor comprising of two α subunits that are associated with ligand binding and two β subunits that mediate the intracellular signaling pathway. The IGF-1R shows approximately 60–85% similarity with Insulin Receptor (IR) in the tyrosine kinase domain (Adams et al., 2000). The binding of respective ligands to the extracellular domain of IGF-1R and the IR results in the autophosphorylation of the tyrosine residue receptors, particularly, Tyr 1158, 1162 and 1163 are important in this regard (Rosen et al., 1983). The IR has two isoforms, IR-A and IR-B. The existence of two isoforms is due to the alternative splicing of exon 11 in the IR, which results in a shorter form, the IR-A form, which lacks a stretch of 12 amino acids and the IR-B form (Mosthaf et al., 1990). The IR-A is associated with fetal tissues and has also been observed in cancer cells. The IR-B is predominantly

associated with the tissues specific for insulin metabolism (Belfiore et al., 2009; Denley et al., 2003). Although the ligands for each receptor are different and are involved in different signaling pathways, there is well established data about binding of IGF-II to the IR-A leading to its activation. Furthermore, there is evidence of a high number of IGF-1R present in transformed cells (Christofori et al., 1994).

Physiologically, the IR is responsible for binding of insulin and should ideally be present in the hepatocytes and the skeletal muscles, but it has been observed that IR is present in other tissues including the brain, heart, monocytes, granulocytes, pancreatic acini, vascular endothelium, kidney and fibroblasts. This observation suggests that IR plays a role not only in the insulin related metabolism but also has functional roles in other systems (Kaplan, 1984). High levels of insulin induce a higher level of serum IGF-I which in turn have properties of mitogen and promote anti-apoptotic behavior in cells. Hence chronic hyperinsulinemia has been associated

* Corresponding author. Faculty of Environment, Society and Design, Lincoln University, P.O. Box: 44000, Lincoln, New Zealand.

E-mail address: mustafa.pasha@lincolnuni.ac.nz (M.K. Pasha).

<https://doi.org/10.1016/j.crchbi.2022.100019>

Received 27 November 2021; Received in revised form 27 December 2021; Accepted 5 January 2022

2666-2469/© 2022 The Authors. Published by Elsevier B.V. This is an open access article under the CC BY-NC-ND license (<http://creativecommons.org/licenses/by-nc-nd/4.0/>).

with carcinogenesis. The IGF-1R is not only involved in the process of transformation of cancers but has also been found to play an important role in the maintenance of the transformed state (Yu and Rohan, 2000).

Over the last two decades, studies have provided in-depth evidence that the IGF-1R is present in various types of cancers and that the blockage of this receptor provides a means of blocking the signaling pathways that follow, particularly the Ras-Raf pathway which is important in providing resistance to the tumors (Benvenuti et al., 2007). IGF-1R is believed to be involved in the proliferation of transformed cells (Yu and Rohan, 2000). As of recent studies, IR-A has also been seen in the course of tumor genesis (Buck et al., 2010). Our previous docking studies on both targets showed that H-bond and hydrophobic pockets play significant roles in initiation of cancer cell cycle (Pashaa et al., 2021). Studies on different myosarcoma cell lines revealed that IR-A is predominantly expressed in sarcoma cells (Sciacca et al., 2002). Most of the cancers express genes for the insulin receptor (IR) as well as the genes encoding Insulin like growth factor 1 receptor (IGF-1R).

One of the key features noted in the expression of IR-A in cancers is associated with its high affinity for IGF-II because of compensatory cross talks between these two receptors leading to signaling pathways that are involved in transformation, cell proliferation and in evading apoptosis (Denley et al., 2004). Targeting IR-A alone would result in hyperglycemia and hyperinsulinemia, leading to metabolic complications (Nemecek et al., 2010).

Since both, the IR-A and IGF-1R (Fig. 1) have been observed in lungs, breast and prostate cancers, there is a need to develop potential inhibitors that could block these receptors and in turn, control the transformation of cells. Previously, monoclonal antibodies have been targeted to block the IGR-IR receptor. Additionally, small molecule inhibitors are being explored for their ability to bind to the receptor to stop the rigorous signaling followed by the receptor binding (Li et al., 2009). In a comprehensive review by Jingran et al., a rationale is discussed for dual inhibition of IGF-1R and IR pointing to importance of dual inhibition (Cao and Yee, 2021). Small molecule inhibitors that can bind to the tyrosine kinase domain have been reported to bind to the catalytic domain responsible for kinase activity (Li et al., 2009; Liu and Gray, 2006a; Zwick et al., 2002). One key approach is to target these receptors in their inactive state because the inactivated ATP binding pocket is less conserved and is a more reliable target. The activated state is conserved among the kinase family and hence proves itself to be a promiscuous target. Therefore, it is a better approach is to target these receptors by

small molecule inhibitors when they are in the inactivated or the DGF-out conformation (Liu and Gray, 2006b). Initial studies revolved around screening and development of small molecule inhibitors against the IGF-1R only but there exist evidence for the role of IR-A in transformation and maintenance of tumors (Buck et al., 2010; Papa and Belfiore, 1996; Baserga, 1995). Targeting IGF-1R alone can have undesirable consequences and may lead to implications that may strengthen malignancies (Christopoulos et al., 2015). A recent study showed the effect of dual inhibitor (OSI-906) on WtU87 cells and concluded its synergistic effect to inhibit IGF1R along with TMZ-40/100 (Fernandez et al., 2019). Along with this, there is increasing evidence that repressing any one of the RTKs (Receptor Tyrosine Kinase) is not enough, the other receptor, still functional, will do enough to compensate and lead to the maintenance and progression of the tumor. Elevated levels of insulin result in higher signaling by IR-A. Also, there is evidence of IGF-II binding to IR-A resulting in an increase in the mitogenic signaling in the transformed cells (Denley et al., 2003). Therefore, a better approach would be co-targeting both the receptors in order to make sure that the mitogenic signaling cascade activated by both these receptors is down-regulated so that proliferative pathways that lead to tumor formations can be stopped (Huang et al., 2015).

2. Materials and methods

2.1. Data set

A diverse dataset of 47 inhibitors, of which; 33 were dual inhibitors of IGF-1R and IR mainly including Imidazopyrazine, Imidazopyridine, Pyrrolopyrimidine, Quinolones, Cyanoquinolines, Isoquinolinedione derivatives (Li et al., 2009; Ji et al., 2007; Jin et al., 2010; Ducray et al., 2011; Mulvihill et al., 2008, 2009; Buchanan et al., 2011; Emmitte et al., 2009; Chamberlain et al., 2009a, 2009b; Miller et al., 2009; Anastassiadis et al., 2013; Mayer et al., 2008; Marsilje et al., 2013; Finlay et al., 2014; Carboni et al., 2009) (Fig. 2) were extracted from the literature and remaining 14 were more selective towards IGF-1R than IR (Liu et al., 2010; Párrizas et al., 1997; Li et al., 2004; Wood et al., 2009). These selective inhibitors against IGF-1R also belonged to the structurally diverse classes i.e Benzylamines, Thiazolidine, Pyrimidine and Ethenylpyridine. Data set of 47 compounds including 'selective' and the 'dual' inhibitors of IGF-1R and IR was used for 3D QSAR and Pharmacophore model building. The 2D structures of the compounds were used in the data set along with their inhibitory biological activity (pIC_{50}) values against tyrosine kinase domain of IR and IGF-1R (Fig. 2). Briefly, the biological activity values of the data vary from 2 nM to 50,000 nM. Compound 40 (Iso propyl Piprazine) (pIC_{50} IGF1R/IR 8.6/8.7) being highly active against both receptors, belonged to the Pyrrolopyrimidine and the least active compound was Isoquinolinedione class. Dataset was divided into selective inhibitors for IGF-1R and dual inhibitors for both targets and were assigned binary numbers. The difference of the IC_{50} s was taken against their target receptors to differentiate them into selective and dual inhibitors for *in-silico* modeling. The optimal threshold of the two halves was pIC_{50} 6.4 nm and 6.2 nm for IGF1R and IR, respectively. While the optimal threshold for dual inhibitors was set 0.6 and those below were considered as selective inhibitors against IGF-1R. In addition to it, Compounds showing the difference of one log unit, or more were considered selective against IGF-1R and assigned "0". While others were considered as dual inhibitors and assigned "1".

2.2. GRID-independent molecular descriptor analysis

GRIND is alignment independent approach; however it depends on 3D conformations of the compounds. Two independent sets of 3D

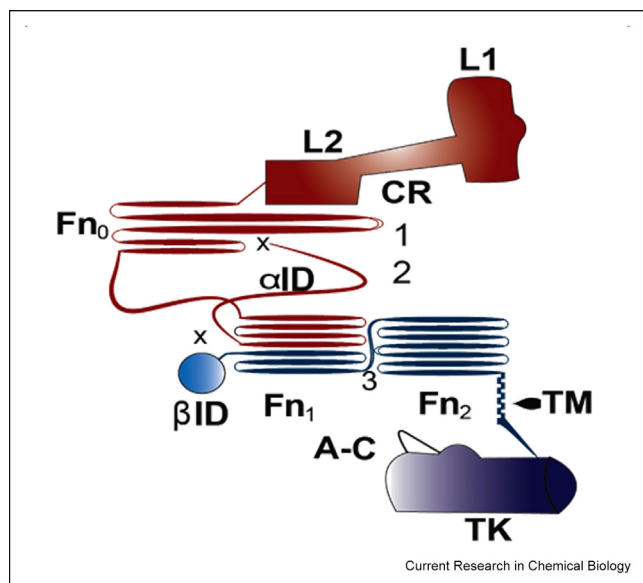


Fig. 1. Structural organization of IGF1R and IR structures adapted from (De Meyts and Whittaker, 2002; Luo et al., 1999; Ottensmeyer et al., 2000).

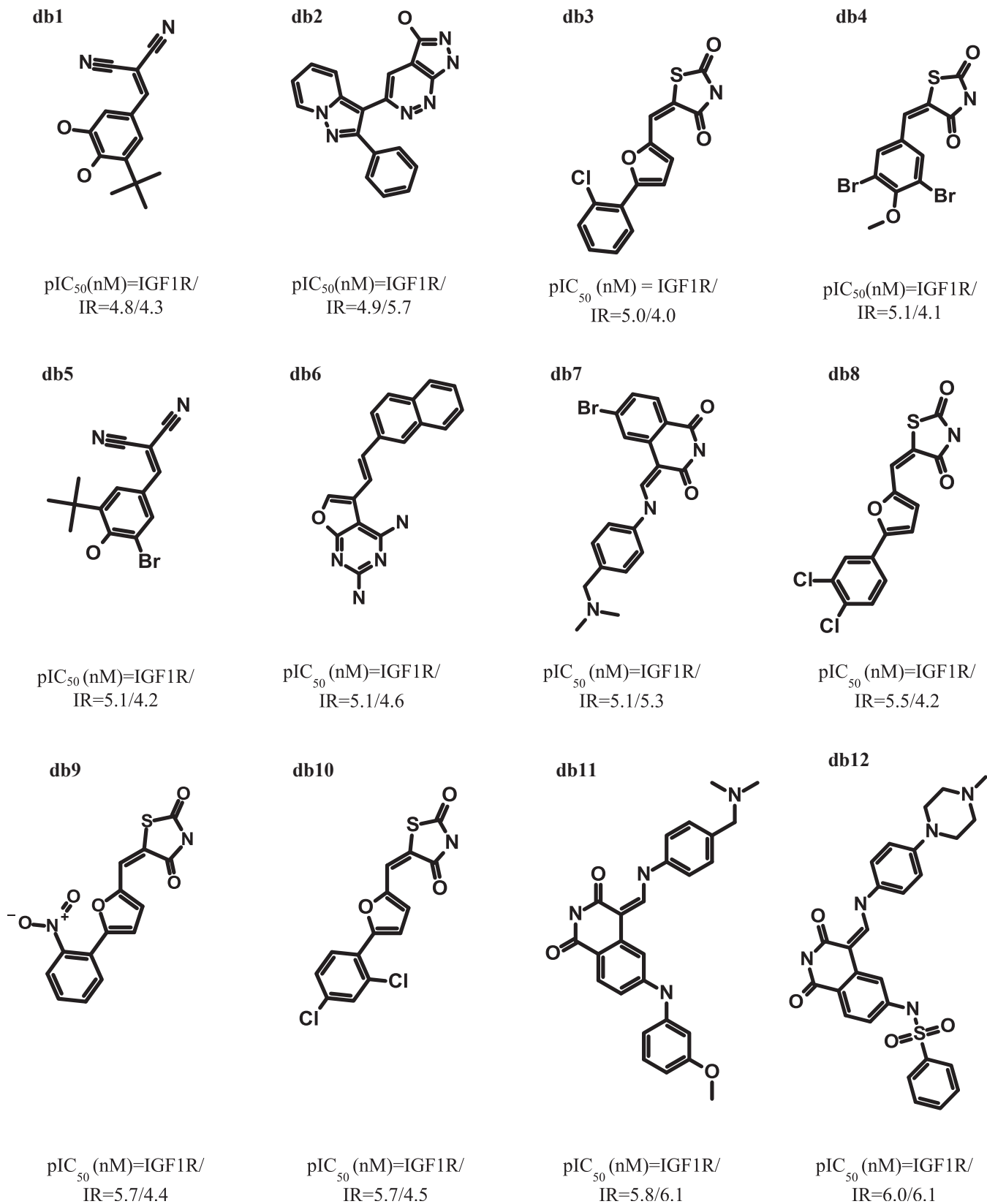


Fig. 2. Database extracted from the Literature.

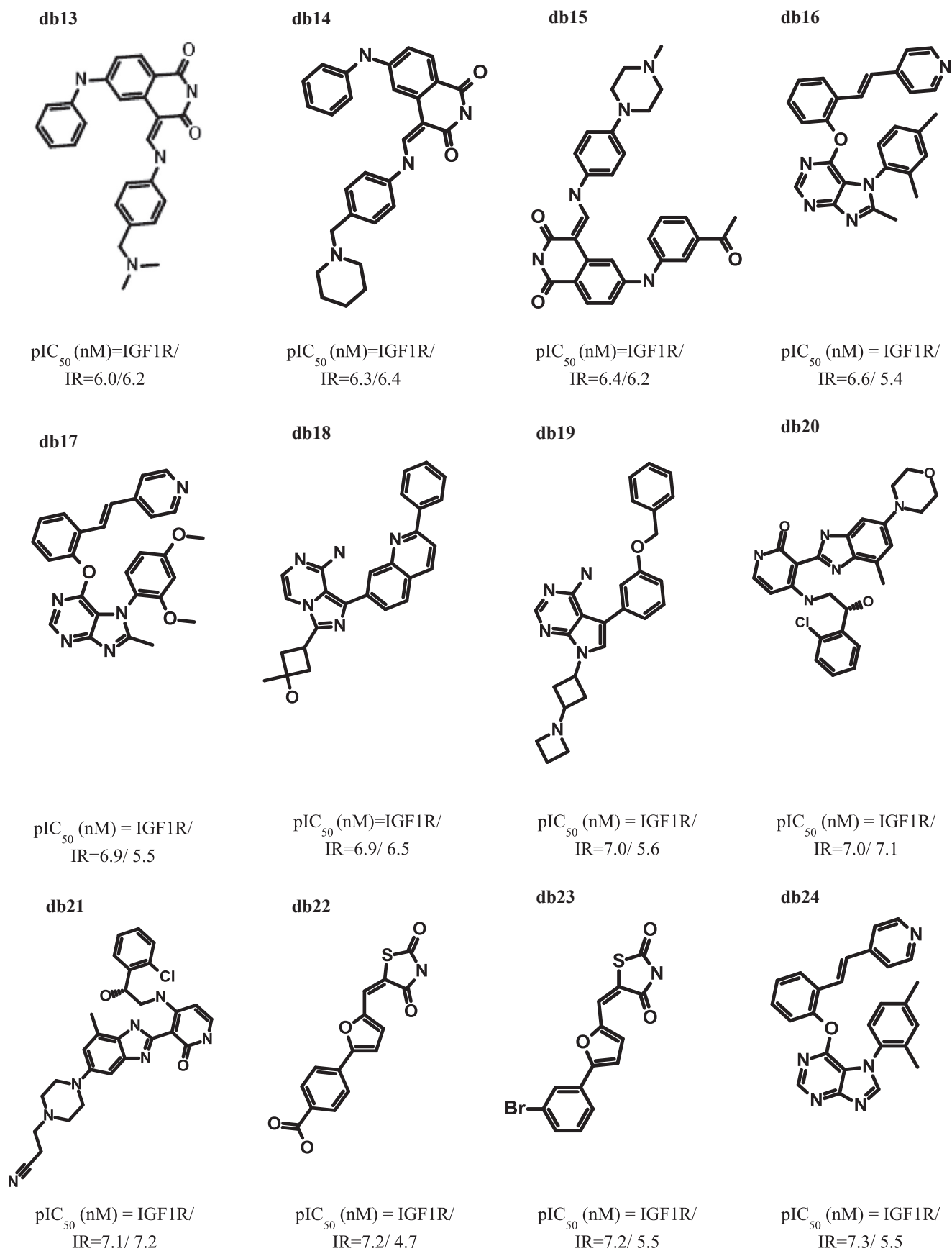


Fig. 2. (continued).

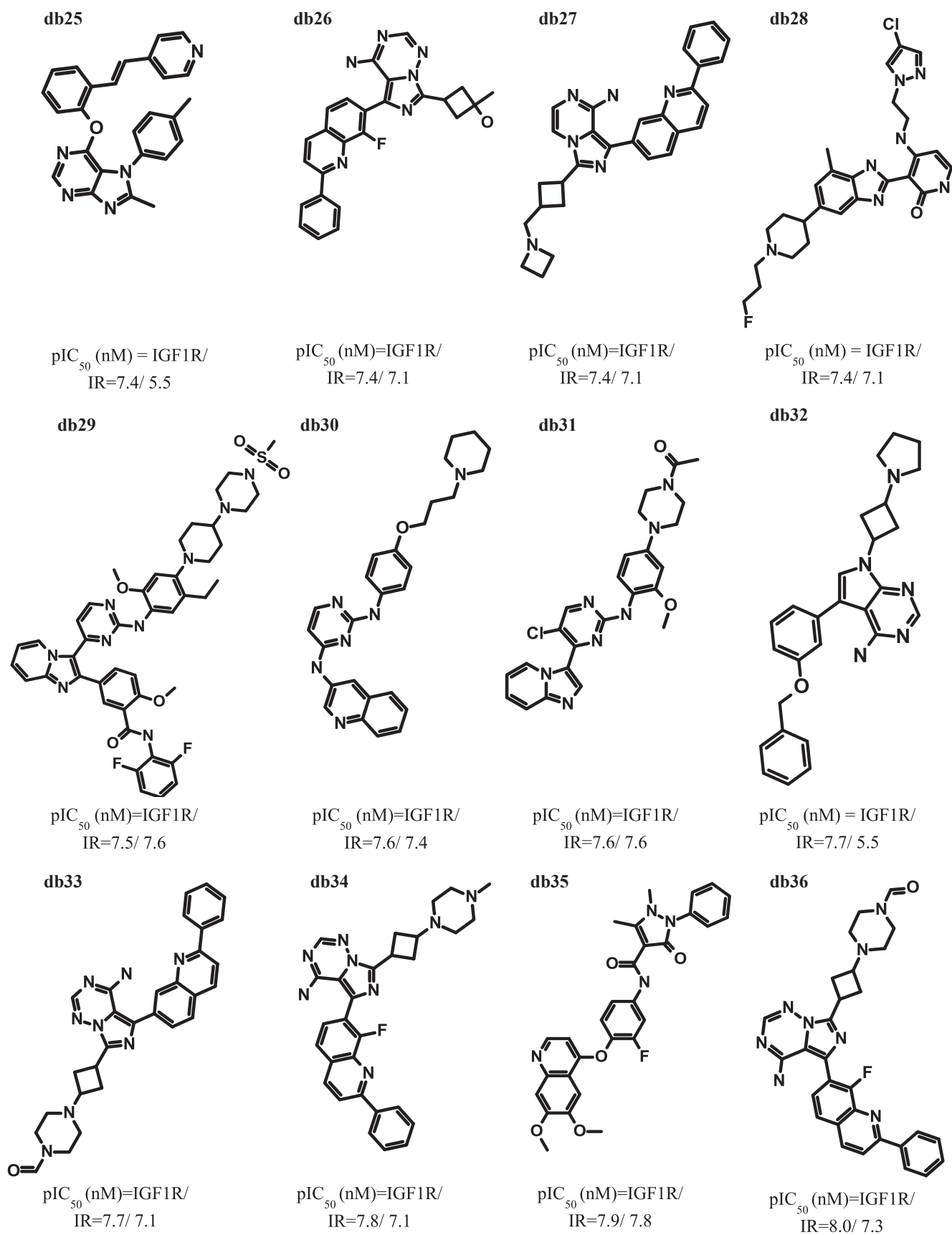


Fig. 2. (continued).

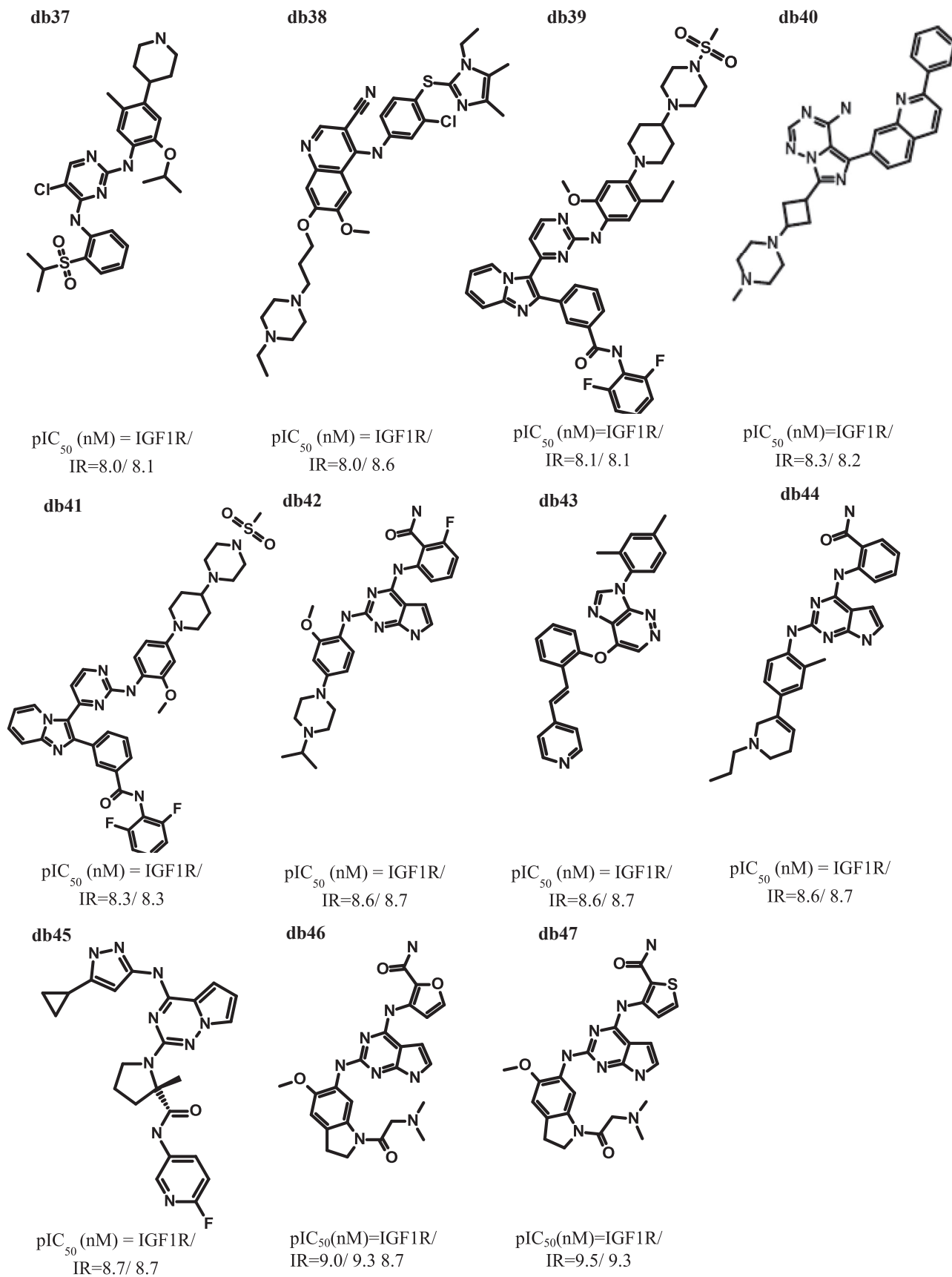


Fig. 2. (continued).

conformations including, energy minimized and extended 3D conformations (Gasteiger et al., 1990; Sadowski et al., 1994) of the data set were used to develop multiple GRIND models. Briefly, minimum energy conformation of each compound in the data set was explored by stochastic search algorithm using the MMFF94 force field in software MOE (Gill et al., 1981). This algorithm (Ferguson and Raber, 1989) divides a molecular structure into overlapping fragments and conformations of molecular fragments are considered independent before the complete assembly of the molecule. Further, it includes the initialization of bond rotations and random inversion of all the chiral centers following Bond rotations to randomized dihedral angles. Later, perturbation of all the atomic positions is done followed by energy minimization. We generated a total of 250 conformations per molecules and out of these only least energy structure per molecule was used for further GRIND analysis.

Additionally, evaluation package “CORINA” (Gasteiger et al., 1990; Sadowski et al., 1994) was used for the generation of extended 3D molecular conformations. Stereochemical information of the molecules was kept fixed to generate low energy conformations via neutralization of formal charges, orientation of the 3D structures with reference to their moment of inertia and removal of counterions in salts. In the following step, each independent set of molecular conformations were imported into Pentacle v 1.07 (Pastor et al., 2000) along with their biological activity values (pIC₅₀). Molecular Interaction Fields (MIFs) were computed using probes i.e., hydrophobic interactions (DRY), Hydrogen bond acceptor (O), Hydrogen bond donor (N1) and Topology representing the molecular boundaries (TIP) with reference to the receptor. These MIFs were calculated by replacing each probe iteratively through the GRID and computing total energy at each node. Total energy at each node represents a sum of Lennard-Jones energy (E_{lj}), electrostatic energy (E_{el}), and hydrogen bond energies (E_{hb}) at that point (Eq. (1)).

$$E_{xyz} = \sum E_{lj} + \sum E_{el} + \sum E_{hb} \quad (1)$$

Most relevant regions were extracted using a built-in algorithm AMANDA (Durán et al., 2008). Default cutoff values for probes were used to discretize the MIFs. Nodes with energy below the cutoff values were discarded. Consistently large auto and cross correlation (CLACC) (Durán et al., 2008) was used for encoding the pre-filtered nodes into GRIND thus, producing consistent sets of variables. The calculated values were represented in the form of correlograms plots representing products of node–node energies on Y-axis and the distances separating the nodes on X-axis. Partial Least Square (PLS) and using Leave One Out (LOO) cross validation procedure was used to correlate structural variance of the data with their biological activity values.

2.3. Pharmacophore modeling

A conformational data set of dual as well as selective inhibitors of IGF-1R and IR containing 250 conformations per molecules were generated from stochastic conformational search algorithm as was discussed in previous section. These conformations were packed and merged with biological activity (pIC₅₀) values against both targets. Both ligands, as well as structure-based pharmacophore models (Sadowski et al., 1994; Gill et al., 1981), were built to develop a binding hypothesis of dual and selective inhibitors of IGF-1R and IR. Finally, this comprehensive database was used for screening against final pharmacophore models to estimate the hit rate and model accuracy.

2.3.1. Model I

Briefly, a highly potent small molecule (NVP-AEW541) (Stauffer et al., 2016) with pIC₅₀ of 7.06 nM against IGF1R, also present in our curated database, was chosen as a template for ligand based pharmacophore modeling. This molecule belonged to a Pyrrolopyrimidine class showing its selectivity 27 times more potent against IGF1R over IR having pIC₅₀ value of 5.63 nM as reported by Frédéric et al. (Stauffer et al., 2016). NVP-AEW541 has been reported for cancer suppression if

co-targeted with autophagy. In a broader sense, it blocks the cell cycle proliferation in G0/G1 phase by cutting the proliferation signal and increasing bax protein concentrations (responsible for apoptosis) and decreasing Bcl-2 protein expressions (Wu et al., 2017). A stepwise pharmacophore feature selection process was performed to extract the most appropriate feature followed by screening against packed training data to identify the true positive and true negative rate. This model delineated 0.68 as overall accuracy for Mathew's correlation coefficient (MCC) (Eq. (2)).

$$TP \times TN - FP \times FN / \sqrt{(TP+FP)(TP+FN)(TN+FP)(TN+FN)} \quad (2)$$

2.3.2. Model II

For a 3D structure based pharmacophore, features were extracted from the ligand bound crystal structure of IGF1R, PDBID: 5HZN (Stauffer et al., 2016), on the basis of receptor binding site algorithm (Wang et al., 2000). A structure-based pharmacophore query was built using information from ligand bound protein interaction profiles of NVP-AEW541. We performed the quality tests for both pharmacophore models and estimated the model sensitivity, specificity, accuracy and the Matthew's correlation coefficient (Chicco, 2017) (Eqs. (2)–(4)). Although, both models successfully parted the data into two halves for selective and dual inhibitors, but structure-based Pharmacophore was utilized for further analysis based on the 0.87 factor MCC.

$$\text{Sensitivity} = TP / (TP + FN) \quad (3)$$

$$\text{Specificity} = TN / (TN + FP) \quad (4)$$

2.4. Virtual screening

In order to identify hits against final Pharmacophore model (structure based) was screened against “World Drug Index” (Wishart et al.) and “ChemBridge” (Groom et al., 2016) databases.

A total of 725 hits from the World Drug Index (WDI) and 19,773 from ChemBridge database were extracted, respectively. The filtered hits were then subjected to online database OCHEM; a CYP filter including different isoforms of CYP450 i.e. CYP1A2, 2C9, 2C19, 2D6, 3A4 and logp to sieve the non-inhibitor small molecules for ADMETox properties, designed by Sushko and colleagues (Sushko et al., 2011). Recently developed Pharmacophoric filter for hERG channels developed by Saba et al. (Munawar et al., 2018) further reduced the number of hits i.e. 143 for WDI and 1540 for ChemBridge. To further screen the hits, drug-like descriptor comparison was executed on the filtered results.

Eventually, binary biological activity values (pIC₅₀) of these hit compounds were predicted using final GRIND model which resulted in 18 highly predicted (pIC₅₀ 0.50–1.21) hits from WDI and 37 (pIC₅₀ 0.50–0.89) hits from Chembridge data based were selected. The compounds predicted near “0” were taken as selective inhibitors for IGF-1R while those which were near “1” were taken as dual inhibitors. For our comparison, the threshold was set to 0.60 for observation against results. Only 4 FDA approved drugs, namely; DB00775, DB01297 and DB09075 were found among which 3 were under-predicted with activity value of 0.62, 0.63 and 0.76 and DB01051 was slightly over-predicted with 1.21, respectively. An MOE based GUI was used to check whether the compounds from the databases to be screened against the Pharmacophore had functional groups required by the pharmacophore or not. Following this, the algorithm checked for the 3D spatial arrangements of these compound that matches the query (Labute and Santavy, 2007).

2.5. Docking

In rational drug design, structure-based drug design is needed. Our objective was to identify the hits from the base protein i.e. IGF-1R kinase (5HZN). On this basis we performed docking on the co-crystalised proteins structures of hits i.e., Beta1-Adrenergic receptor, PDBID: 7JJO (Su

Table 1
Energy minimized and extended statistics.

Conformations	R2	Q2	SDEP	FFD/ LV
Energy min	0.89	0.54	0.10	1/ 3
Extended	0.61	0.33	0.22	0/2
	0.65	0.45	0.24	1/2
	0.76	0.60	0.37	2/2

SDEP = Standard error prediction. FFD = Factorial Design. LV = latent variable.

Table 2
Important Distances by GRIND; Representation of distances from having negative effect (larger distance) to positive effect (closer distance) on the macromolecule.

Features	Important Distance (Å)
N1–N1	12.8–13.2
DRY–O	19.2–19.6
DRY–N1	18.4–18.8
O–N1	14.8–15.2
O–TIP	18.4–18.8

et al., 2020) and Integrin Beta-3 and integrin alpha II-B, PDBID: 6BXJ (Thinn et al., 2018). The idea of structure-based docking was to gain insights into electrostatic and steric hindrances of the hits and declaring the crucial amino acid connections.

Dock application from MOE was used to produce optimal fit configurations of the inhibitors and macromolecular target (5HZN, 7JJO and 6BXJ). The first choice for docking was to perform runs consecutively with each member of the ensemble by using rigid receptor docking. The dock algorithm (Chamberlain et al., 2009a) automatically generated 3D conformations which seemed to fit optimally into the pocket with the help of “Placement method” for ligand placement.

We've shown a structural comparison of the crystallographic receptors (Table 9). Afterwards we matched the pocket residues and did loop comparison. For the comparison, these structures were aligned with blossom62 matrix-based calculation, where root mean square deviation (RMSD) was performed. Moreover, it was also considered whether the Co-crystal structures were recently published and had higher resolution.

The placement methods used in the optimization of protocol were, Alpha Triangle, Triangle Matcher and Alpha PMI. We then scored the poses after the placement of the ligand into the pocket with a stress on favourable ionic, hydrophobic and H-bond contacts. Later, scoring functions were used i.e., London dG Scoring, Affinity dG Scoring and Alpha HB Scoring. Upon testing several combinations of placement methods and scoring functions for docking, Alpha PMI and Alpha HB were considered final for further dockings and analysis. Once Docking

runs were performed, the generated databases of optimal conformations for bioactive interactions between molecules and receptors were further analysed for amino acids involved in interactions and important features of the ligands.

3. Results

3.1. 3D-QSAR

The independent set of molecular conformations (standard 3D conformations and energy minimized conformations) along with binary biological activity values (“0” for selective against IGF-1R and “1” for dual against both IGF-1R and IR) were subjected to software Pentacle V1.07 to develop two independent GRIND models. Statistical parameters of both models are shown in Table 1.

The model based on the standard 3D conformations showed better r^2 and q^2 better than those of energy minimized conformation model. The Latent variable “2” shows a measure of confidence that the hidden information with twice a fractional analysis of the variable data is delineating a good statistics score of $r^2 = 0.76$ and $q^2 = 0.60$. Among four probes; Dry–Dry (Hydrophobic), O–O (H- bond acceptors), N1–N1 (H- bond donors), Tip- Tip (Topology) and also their intercross distances and energy scores delineated 4 important distances and descriptors shown in Table 2.

The overall trend seen for H-bonding relied on the electronegativity of the atoms. Atoms i.e. Sulphur, Chlorine, Boron, Fluorine have shown least inclination towards H- bonding except the fact that fluorine is most electronegative. We presumed that the power of an electronegative atom to donate a H- bond depends on its overall topology and van der waal forces. Both of these descriptors have played their role in the overall positive and negative impact. Also, In comparative analysis with previous published reports (Muddassar et al., 2008; Sperandio et al., 2009; Kurup et al., 2001; Sheridan et al., 2009; Li et al., 2012) our preliminary models remained consistent with electrostatic potential and hydrophobicity except steric bulk. The final model has revealed steric bulk along with H-bond donor; O- TIP play a pivotal role at a distance of 18.40–18.80 Å along with previously stated descriptors (Fig. 3). In line with steric and electrostatic descriptor, two sets of O–N1 and N1– N1 probes imparted their presence as obligatory variables at the distance of 14.80–15.20 Å and 12.80–13.20 Å, respectively (Fig. 3). Clearly, the N1–N1 probe's distances from pyridine ring to phenyl ethanol moiety showed a promising impact for compound 4a based on the least distance of 12.80–13.20 Å and the highest peak in the correlogram depicting the positive contribution towards the dual inhibition. While, no such distance could be found in selective inhibitors against IGF-1R, showing the absence of such functional groups. The second most active dual inhibitor

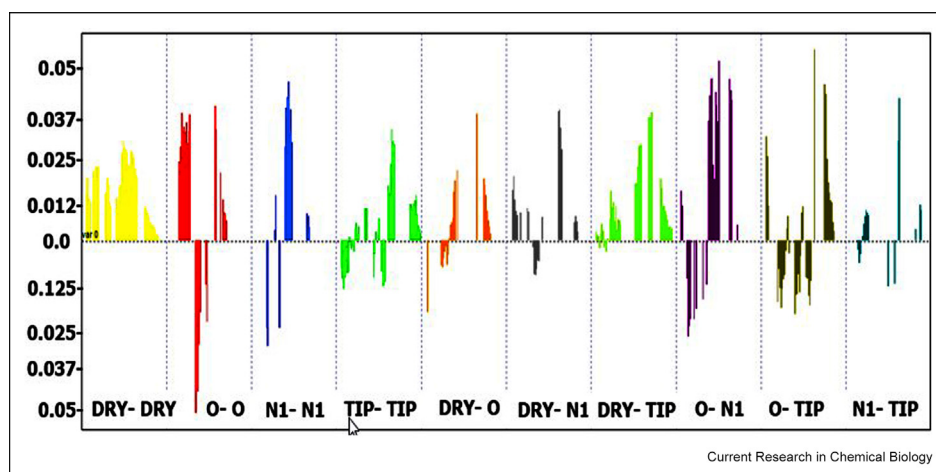


Fig. 3. GRIND Correlogram delineating important variables O–O, N1–N1, O–N1 and O–TIP.

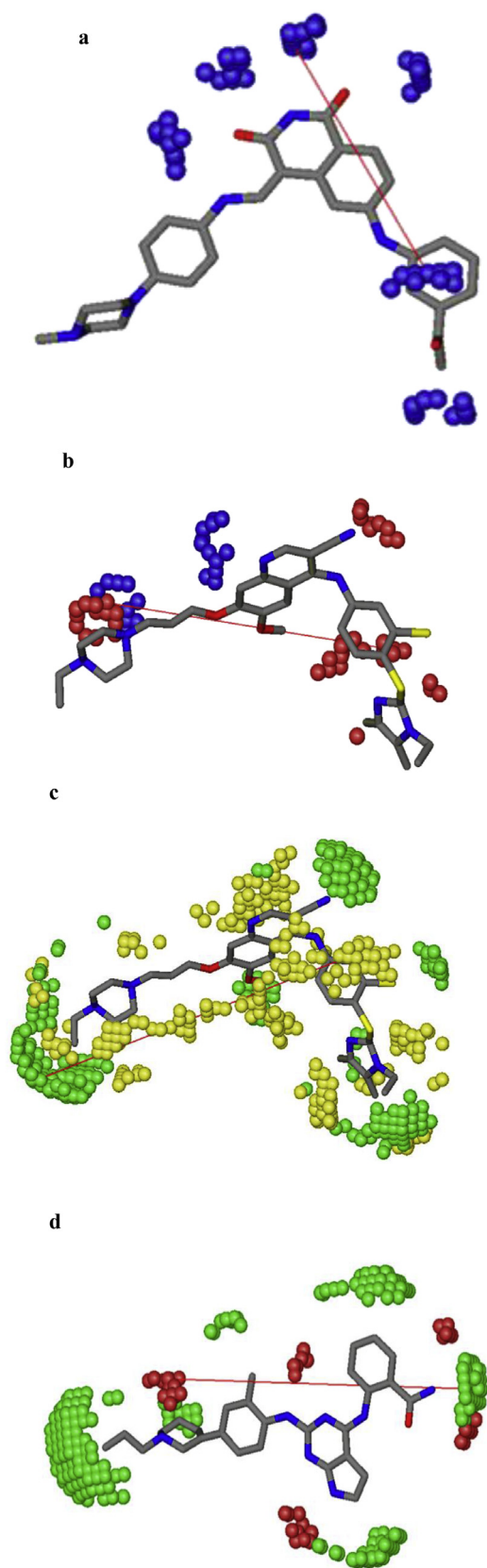


Fig. 4. The PLS coefficient GRIND correlogram identified regions for Dual Inhibition described by visual receptor site. a; Distance between two H-bond acceptor (blue contours) b; Distance between H-bond donors (red) and acceptor (blue), c; larger distance found between nodes of bulk (green) and Dry (yellow), d; Optimal distance between H-bond donor (red) and steric bulk (green). For reference see Table 2.

showed the same probe distance between pyridine moiety and pyrazolidine ring. Also, the third one with another electronegative moiety as Florobenzene. Similarly, the O–O probe (Fig. 3) have delineated the optimal distances between the pyridine ring and methanolamine in compound 4b for selective inhibitors against IGF1R only. Along with this, O–N1 showed affinity with imidazolidine and pyrazine in compound 4b. Also, the DRY-TIP showed the same potential with similar groups with addition of chlorothiophenol moiety as hydrophobic ring 4c. Lastly, O-TIP showed the methanolamine and pyridine moieties as an important bifunctional group for dual inhibition of the small molecule 4d. Upon visual analysis of the graph, the variables representing the true nodes of these four probes with moieties like pyridine, pyrazolidine, methanolamine are considered as playing crucially important role in the dual inhibition of both receptors. While, a lesser distance or no distance could be found between such probes in selective inhibitors.

The consistency with previous models was taken into account by variable sets of DRY- N1 which happened to be present at the distance of 18.00–19.20 Å. While O–N1 (Fig. 4c) and O-Tip (Fig. 4d) at distance of 18.4–18.8 were found concurrently, have also contributed positively towards the inhibitory trends for dual inhibition.

3.2. External validation

A test set of 20% of the total data extracted from the literature was utilized against the validation of the curated database. The test set was non-congeneric and IC_{50} values ranged from 2 nM to 20,000 nM against IGF-1R and IR. The results delineated high consistency course along the training set in terms of dual or selective inhibition. Except **Compound e**, no outliers were found against the level 2 prediction of GRIND model built against 3D standard conformations.

3.2.1. Test Set I

The data extracted was dual as well as selective in nature against IGF-1R having at least one log unit difference with respect to IR i.e. compound **d f, h, i, j** (Fig. 5). The test set contained almost the same percentage of selective and dual inhibitors of both receptors i.e. 40% selective and 60% dual. Predictions of test set based on the GRIND model distinctive features were within the binary range of training set. Those predicted near 1 were considered as dual. While inhibitors having the predicted values near 0 were taken as selective inhibitors of IGF-1R. Among the data only compounds **a** and **g** were under-predicted and compound **e** was slightly over-predicted (Table 3).

3.2.2. Test set II

Recently published data along with a clinical trial candidate was also extracted and used as an external test set for the model validation (Hempel et al., 2017; Sabari et al., 2017; Wang et al., 2017) (Fig. 6).

A total of 12 compounds were distinguished as selective and remaining 6 as dual (Tables 4–5). Dual small molecule inhibitors assigned '1' were called test set 2 (Table 4). When the validations were run against the GRIND model based on standard conformations, This test set II showed predictions near 1. This further strengthens the findings that the predicted values are true to their very nature of molecules.

3.2.3. Test set III

The test set III having IGF1R selective inhibitors (Table 5) showed selectivity predictions against IGF-1R. Those lied near or below zero were considered as selective against IGF-1R receptor (Table 5). No outlier were observed. There is no evidence found yet for the duality of these compounds including literature. This strengthens our finding while cross checking the trend for duality. From the predictions of test set III designed for IGF1R, the interaction pattern was similar with our Pharmacophore model. Most interestingly, these analogues contained all those electronegative functional groups and atoms which were predicted by 3D GRIND model. The overall statistics (q^2 and r^2) of the Test sets was >0.5 which further signifies the external validations.

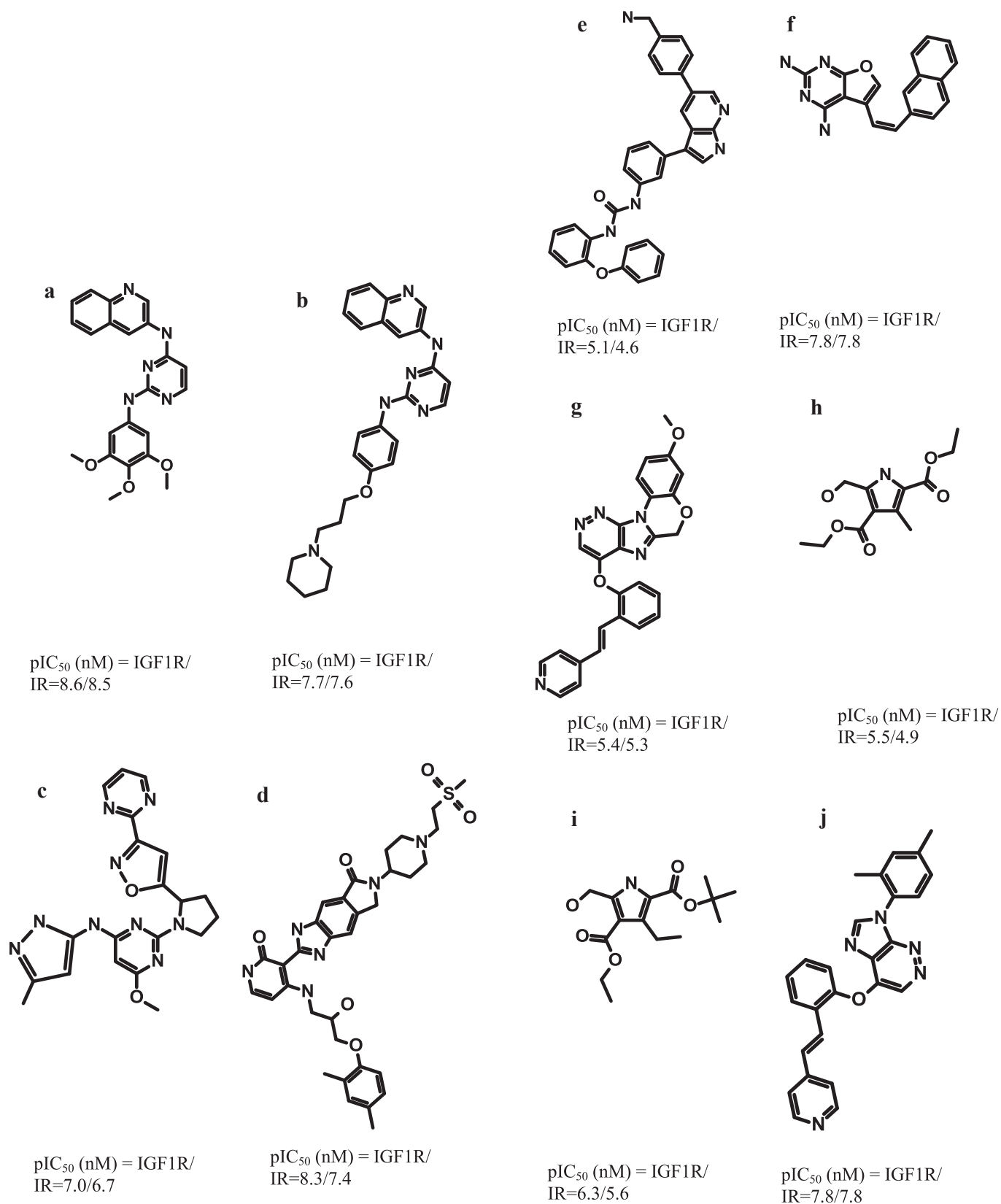


Fig. 5. External Data set extracted from recent literature.

Table 3
Predictions on External Validation set 1.

Molecule	Selectivity	LV 2 Prediction	Difference
Comp a	1	0.34	0.65
Comp b	1	0.75	0.24
Comp c	1	1.08	-0.08
Comp d	0	0.15	-0.15
Comp e	1	1.50	-0.50
Comp f	0	0.13	-0.13
Comp g	1	0.42	0.57
Comp h	0	0.05	-0.05
Comp i	0	0.06	-0.06
Comp j	0	0.28	-0.28

Table 4 shows the statistics predicted by the GRIND model for the validation of compounds which were considered to be dual inhibitors for IGF1R and IR. The predictions were built on the training set obtained via extended conformations. Similar threshold was designed for such data where dual inhibitors were termed as 1. The prediction clearly identifies the behavior towards the inhibition of both Targets. It could be delineated that these compounds would interact in similar fashion as of those upon which training set was built. The predictions, near 1 also evidently support the hypothesis build by 2D and 3D QSAR.

Each study was in line with previous research results. The electro-negativity of the atoms at the extremities of the molecules *i.e.* Fluorine and phosphate group of Brigatinib and Comp 19 have made them to be predicted as potent dual inhibitors of Tyrosine Kinase inhibitors. On the other hand Comp HKI272(2) has been over predicted (Table 4).

3.3. Pharmacophore modeling

As described above, structure and ligand-based pharmacophore models were generated. The 3D coordinates of co-crystallized structure of IGF-1R (5HZN) were downloaded from protein databank having NVP-AEW451. Based on Mathew's correlation coefficient (Eq. (2)), structure-based pharmacophore was chosen. This model successfully parted the data with one false negative and 2 false positives. The overall accuracy of the system was 0.87.

Typical pharmacophoric features were built against abstract conformations *i.e.* hydrophobic centroids, Aromatic rings, H-bond acceptor, H-bond Donor, Cations & Anions. These features define the fate of eliciting pharmacological actions for various responses.

3.3.1. Model I (ligand-based pharmacophore)

The first model built on NVP-AEW541 efficiently marked the most potent inhibitors of dual inhibitors. Despite having a good Mathew's correlation factor of 0.68, it was clear from the analysis that this model failed to produce any reliable result. The reason for choosing NVP-AEW541 was its co-crystal structural importance that demonstrated several key interactions and also its presence on the threshold of dual and selective inhibitor. The model contained two H-bond acceptors with the radius of 0.9 Å and 1.6 Å and two HYD|ARO and H-bond donor with a radius of 1.4 Å and 1.3 Å respectively. When this pharmacophore model was screened against the abstract information obtained from the stochastic search with the threshold of 150 nM inhibitory concentration, The abstract conformation was unpacked later to procure energy minimized conformation to utilize them for GRIND models which failed to produce matching results. Although, previously published reports (Liu et al., 2010; Taha et al., 2007; Ramdhare and Nandave, 2016) have completely matched with the present pharmacophore model irrespective of the numbers of the pharmacophoric features. Unlike published reports, our model failed to correspond to negative ionizable feature.

3.3.2. Model II (structure-based pharmacophore)

In structure-based pharmacophore (Fig. 7), NVP-AEW451 had a strong H-bond interaction with LYS 1030 where it accepted an H-bond

from the side chain of 5HZN. On the other hand, hydrophobic interactions with the benzene ring could also be seen. GLU 1077 was a backbone H-acceptor and MET 1079 as H-donor along with ASP 1083 as H-acceptor. It was hypothesized that the inhibitors from the database bind in a similar fashion with the receptor, then common group (features) could interact with the same protein residue.

This information was extracted from the region defined by the automated program. A similar fashion of search for hits and model assessment was performed as it was executed on ligand-based pharmacophore. The structure-based Pharmacophore revealed that there could exist pie-pie interaction between the terminal benzene ring of NVP-AEW541 and LYS1030. Rest of the denouncements were in line with the proposed Pharmacophore. The distance comparison is shown in Table 6, where we compared the inter-feature distances.

One of the reviews by pakaj et al. also identified similar feature for different small molecules to be dual inhibitors.

3.4. Virtual screening

The structure based Pharmacophore generated was screened against World Drug Index (WDI) and ChemBridge databases (Wishart et al.; Groom et al., 2016) having 6.5 thousands and 0.45 million entries respectively. Since, the chosen pharmacophore was structure based, the interaction patterns explained in pharmacophore and GRIND section were the key indicator that the filtered candidates from the databases would have dual inhibition characteristics of both receptors. Based on traditional lock and key model, results from pharmacophore model and Mathew's correlation delineates that the hits from WDI and ChemBridge databases have the same pharmacophoric feature which would help them bind the stated receptors and block proliferation signal. It is evident from the statistics; number of Pharmacophoric features and distances that structure-based pharmacophore was the right choice for virtual screening. The hits obtained via virtual screening filtered 725 candidates from World Drug Index and 19,773 from ChemBridge data base as dual inhibitors.

This also validates the results generated by GRIND model. The selective and dual inhibitors separation of the external test sets delineates the authenticity of the pharmacophoric model. The compounds predicted by GRIND near "0" were taken as selective inhibitors for IGF1R while those near "1" were taken as dual inhibitors. The column of LV 2 shows the predicted values of the WDI drugs against their inhibitors. All the entities in this table are above 0.5 which are considered to be active against dual receptors as they are predicted near one (Table 4). For our comparison, to tighten the criteria, we increased the threshold to 0.60 and scrutinized the results which revealed only 4 FDA approved drugs. Among them DB00775, DB01297 and DB09075 were under-predicted with 0.62300003, 0.63910002 and 0.76560003 respectively, while DB01051 was slightly over-predicted with 1.2187999 (Table 7) at LV 2 upon which GRIND model relied.

The compounds having FDA approval are considered final hits and therefore recommended for further analysis. They satisfy atomic count, Molecular weight, and other properties for a drug like entity.

3.5. Pharmacophore modeling of hits proteins

To produce efficient results, we chose the stringent criteria to be applied on docking. Only those proteins were chosen which had PIC₅₀ value closer to 0.6. To obtain all available chemical information on the hits' binding of 7JJO and 6BXJ, two different structure-based Pharmacophore models were constructed. We used the co-crystallized ligand from 5HZN structure in order to build pharmacophore which would depict true features as our base pharmacophore. Similarly, we used Eqs. (2)–(4) for the correlation coefficient, sensitivity, and specificity, respectively. We found that our model with Beta1-Adrenergic receptor (7JJO) showed 79% significance confirming that it is well predicted (Fig. 8). Similarly, our model with Integrin Beta-3 and integrin alpha II-B

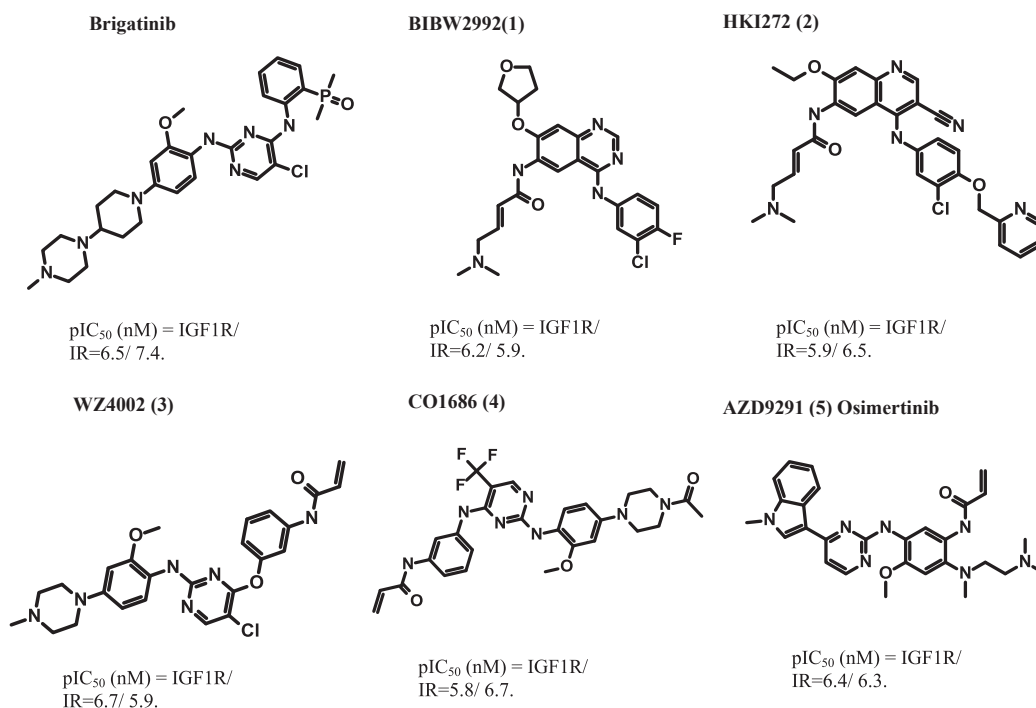


Fig. 6. External validation data set with pIC_{50} values *the difference of 1 log unit can be seen.

(6BXJ) had 79% MCC accuracy (Fig. 9). Both models predicted similar features with a much lower distance than our base model. All three models, including the base model, evidently distinguish the active and inactive compounds. We believe that these will provide deeper insights into the ligand binding at the binding domain by mapping the mutual distances of important pharmacophore features that interact with amino acid residues.

These models were consisted of similar features including hydrophobic feature with Aromatic feature (F1: Hyd|Aro), aromatic feature (F2: Aro), hydrogen bond donor feature (F3: Don), and hydrogen bond acceptor feature (F4: Acc). The overall range of the radius was within 0.5–2.0 Å. We've shown a comprehensive distance and RMSD comparison in Tables 8 and 9, respectively, where we can see similar patterns not only in distances but also in RMSD of these target structures.

Table 4
 Predictions for External test set 2.

Comp.	Experimental pIC_{50} -IG1R	Experimental pIC_{50} -IR	Actual/ Selective (Dual)	Calc./ Predicted pIC_{50} -IGF-1R
Brigatinib	6.58	7.42	Dual 1	Dual 1
BIBW2992(1)	6.25	5.92	Dual 1	Dual 1
HKI272 (2)	5.92	6.53	Dual 1	Dual 1
WZ4002 (3)	6.72	5.92	Dual 1	Dual 1
CO1686 (4)	5.88	6.72	Dual 1	Dual 1
AZD9291 (5) Osimertinib	6.44	6.30	Dual 1	Dual 1

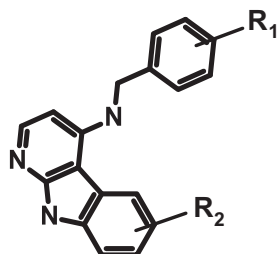


Table 5
 Predictions for external test set 3.

Comp.	R ₁	R ₂	Experimental pIC_{50} -IGF-1R	Actual Selectivity/ Selective	Calc./ Predicted pIC_{50} -IGF-1R
5a	3-OMe	p-Br	5.00	Selective 0	Selective 0
5b	3-Cl	p-Br	5.45	Selective 0	Selective 0
5c	3-BR	p-Br	5.52	Selective 0	Selective 0
5d	3-NH2	p-Br	6.27	Selective 0	Selective 0
5e	4-OMe	p-Br	5.65	Selective 0	Selective 0
5f	4-Cl	p-Br	5.64	Selective 0	Selective 0
5g	4-Br	p-Br	6.05	Selective 0	Selective 0
5h	4-Me	p-Br	6.15	Selective 0	Selective 0
6a	3-OMe	p-CN	6.54	Selective 0	Selective 0
6b	4-OMe	p-CN	6.57	Selective 0	Selective 0
6c	4-Me	p-CN	6.40	Selective 0	Selective 0
7	3-OMe	p-COOH	5.62	Selective 0	Selective 0

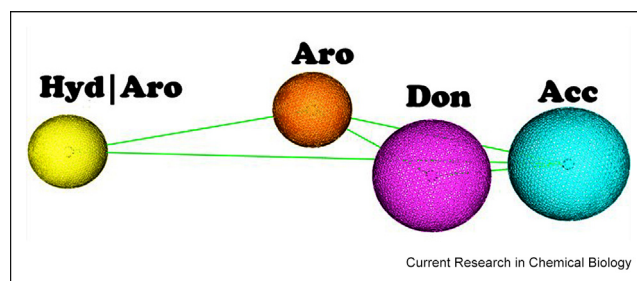
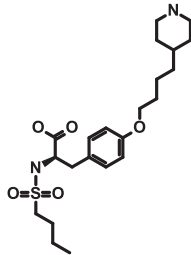
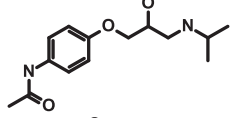
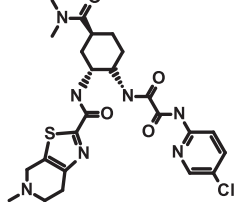
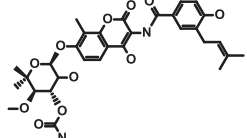


Fig. 7. Pharmacophore built against extended database.

Table 6
 Distances of descriptors on 5HZN.

	Hyd Aro Å	Aro Å	Don Å	Acc Å
Hyd Aro	–	5.10	7.56	10.30
Aro	5.10	–	2.82	5.31
Don	7.56	2.82	–	2.77
Acc	10.30	5.31	2.77	–

Table 7
Finalized Compounds (hits predicted by GRIND model) for future investigations.

Generic Names	2D- Structure	Predicted pIC ₅₀	Class	Target	Indication
Tirofiban		0.62	Phenylpropanoic acids	Integrin β -3 & Integrin α -IIb	Acute Coronary syndrome
Practolol		0.63	Acetanilides, Benzenoids	Beta-1 adrenergic receptor	Cardiac Arrhythmia Emergency Treatment
Edoxaban		0.76	Novel Oral Anti-Coagulants (NOACs) class of drugs	Coagulation Factor X	Stroke risk and systemic embolism in patients with non-valvular atrial fibrillation (NVAf)
Novobiocin		1.21	Coumarin Glycosides	DNA Gyrase sub Unit B & DNA topoisomerase 1	Infections due to Staphylococci and other susceptible organisms

3.6. Docking on hits' proteins

Simulation of Molecular docking was executed with the aim to predict the most favorable ligand-target spatial configuration as well as to visualize the binding of these ligands to the active site to get each conformation's native binding. Hydrogens were added, partial charges were computed, and energy minimization was performed using Amber99 force field (gradient: 0.05). Docking of Practolol and Tirofiban with 5hzn was performed through MOE 2017.100 poses of each ligand were generated with the combination of scoring function Alpha HB and placement methods Alpha Triangle to check the behaviour of ligands in the binding site and also to observe native binding site through the docking.

Practolol docked in 5HZN shows hydrogen bonding with Met1076,

Met1079 and Asp1150 that was already reported by the previous docking studies related to the IGF-1R (Su et al., 2020). Another potential target Tirofiban docked in 5HZN also shows the same hydrogen bonding with Val1010 and Met 1076. These results demonstrated that both potential targets show the same interaction pattern and have the potency to inhibit the IGF-1R.

For protein profiling, the co-crystallized ligand of 5hzn was docked in hits' proteins and protein ligand interaction analysis was performed (Table 10). The results show that the same interaction pattern as the native interaction pattern of proteins was observed. Also, the hydrogen bond interaction with most effective amino acid of the protein can be seen in Table 10. Beta1-Adrenergic receptor (7JJO) docked with NVP derivative shows the importance of hydrogen bond interaction by pairing with Phe306, and similar hydrogen bond interaction were seen with Integrin Beta-3 and integrin alpha II-B (6BXJ) i.e., Asp95, Glu337, Ser306 and Asn308. These results demonstrated that hydrogen bonding is important for the inhibition of the hit's protein.

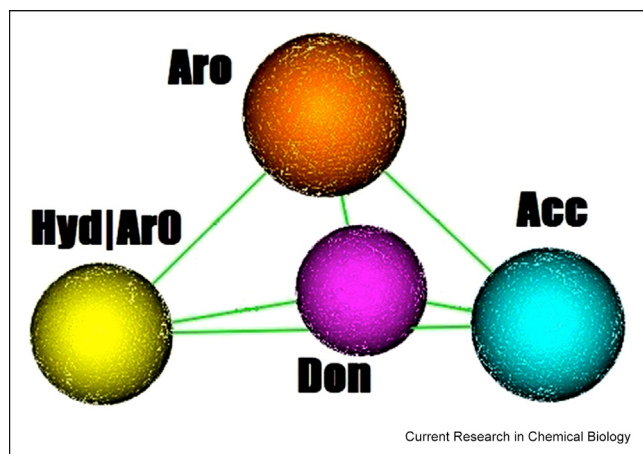


Fig. 8. Beta 1 adrenergic receptor structure based pharmacophore.

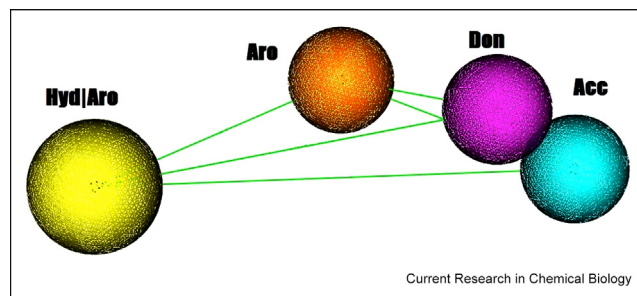


Fig. 9. Integrin Beta-3 receptor structure based pharmacophore.

Table 8

Radius & Distances Comparison of Hits' proteins.

Features	6BXJ					7JJO					5hzn Base Structure				
	Radius	Hyd/Aro	Aro	Don	Acc	Radius	Hyd/Aro	Aro	Don	Acc	Radius	Hyd/Aro	Aro	Don	Acc
Hyd/Aro	1.50	–	5.41	4.43	6.21	1.30	–	6.67	4.60	3.59	0.8	–	5.10	7.56	10.30
Aro	1.20	5.41	–	3.99	5.36	1.20	6.6	–	32.38	3.29	0.8	5.10	–	2.82	5.31
Don	1.20	4.43	3.99	–	2.38	1.40	4.60	238	–	3.59	1.2	7.56	2.82	–	2.77
Acc	1.20	6.21	5.36	2.38	–	1.50	3.59	3.29	3.59	–	1.2	10.30	5.31	2.77	–

Table 9

Structural comparison of hits protein with IGF-1R kinase (5HZN).

Protein Name	RMSD with IGF-1R (5HZN) (Superimposed structure only)
Beta1-Adrenergic receptor (7JJO)	2.864 (40 residues)
Integrin Beta-3/Integrin alpha II-B (6BXJ)	3.02 (34 residues)

Table 10

Important Amino Acid: Hits docked in 5HZN.

Ligands	Interaction Type	Amino Acid Involved
NVP-Derivative	H- Bond Donor & Acceptor	Gln1004, Glu1077, Met1079, Arg1136, Val1010, Met1076,
Practolol	H- Bond Donor & Acceptor	Met1076, Asp1150, Met1079
Tirofiban	H- Bond Donor	Val1010, Met1076

4. Discussion

The current study offers robust investigative protocols for potential clinical candidates. We confirm that the Pharmacophore and GRIND models concurrently delineate two H-bond donors, two H-bond acceptors, overall Topology and vdW_vol as important descriptors for dual inhibition of IGF-1R and IR.

Our GRIND model showed two H-bond donors at the distance of 16.8–17.2 Å and two H-bond acceptors at the distance of 12.8–13.2 Å respectively. It also predicted that steric bulk along with H-bond donor at 18–22 Å plays a significant role in the affinity. The partial least square analysis with latent variables and factorial design from Final GRIND model gave an $r^2 = 0.76$ with a cross validation $q^2 = 0.60$, reflecting statistically significant results. Additionally, external validation performed with three external test sets for selective and dual inhibitors from published research reflected the model results. Furthermore, our pharmacophore model delineated the distances between the descriptors like hydrophobic region, H-bond acceptors and donor region to be important. Moreover, a strong Mathew's correlation factor of 0.87 from our pharmacophore model was obtained, which suffices the significance of the model. Lastly, model query against WDI and ChemBridge resulted in potential hits for dual inhibition of both IGF-1R and IR.

Herein, the models and virtual screening reveals crucial distances among H-bond donors and acceptor and overall topology. From the final hits, the Edoxaban possesses a pair of hydrogen bond acceptors present at 13.5 and 15.5 Å. Likewise, for over-predicted candidate Tirofiban, the distance found is approximately 18.4 and 12.6 Å, which is promising based on our predicted distances from the GRIND model. The identified features and distances are paralleled in both models, witnessing the intrinsic dual inhibitory nature of the compounds. Recent studies are either suggesting correlated potentiation of dual inhibition of IGF-1R and IR with cytoskeleton actin-binding protein filamin A (FLNA) inhibition or chimeric modified receptor (Catalano et al., 2021; de Billy et al., 2020). We further confirm the accuracy of the models through Docking and pharmacophore models on hits' target proteins, which delineated similar features and amino acids as the base model with accuracy of 79%. These

further hints the candidacy of the NVP derived pharmacophoric model and potential hits from QSAR studies. Hence, in the absence of experimental data available and on the bases of diverse and non-congeneric chemical classes, our models and validations provide statistically significant results upon which further research and experimentations can be performed for repositioning of drugs.

5. Conclusion

The compensatory cross-talks occurrence upon inhibition of IGF1R and high sequence homology between the binding domains of IGF1R and IR pave the idea of dual inhibition of both receptors. This led to a race in novel molecular agents' experimentation and dual targeted inhibition through cutting edge techniques. The purpose of using *in-silico* should address the drug resistance, toxicology, and other complication. Even though recent studies have given us a small degree of confidence, yet precautions should be exercised while modeling the ADMETox properties and performing repositioning of the drugs. Among recent discoveries, first in human phase clinical trials candidate KW-2450 showed hyperglycemia and hyperinsulinemia concluding more research is needed in this area (Umehara et al., 2018), along with other leading dual inhibitors to date i.e. Linsitinib (OSI-906), GSK and NVP derivatives, and Erlotinib. This study will help in the evaluation the ligand efficiency. We have thoroughly researched the Pharmacophore models and confirmed through high throughput screening and the cross validations that the NVP- derivatives can be potential clinical candidates. Additionally, previous models were solely based on exploring unaccompanied solo properties, i.e., modeling of a single class 2D or 3D, or in some cases the delineated features were limited.

The ADMETox studies on these novel molecules would additionally explore the possibility of their clinical candidacy. Further optimization and experimental validation of identified hits will pave a way towards the successful development of chemotherapeutic agents against difference types of cancers. For example, the optimization of classes including Thiazolidinedione (TZD) or pyrimidines have led to the discovery of potent novel molecules.

However, strong computational tools with advanced A.I and machine learning algorithms are needed in the drug discovery process. The experimental validations for each computational study performed on cell lines may provide further insights onto the chemical nature of the molecule, including the ligand efficiency and profiling. Current findings encourage a promising window into cancer research and could aid into the development of potential clinical candidate.

Software availability

- 1 To obtain MOE commercial Software for reproduction purposes, please request at https://www.chemcomp.com/Contact.htm?q=trial_request&interest=Molecular%20Operating%20Environment.
- 2 To obtain Pentacle software for review purposes please locate at <https://www.moldiscovery.com/software/pentacle/>.

Funding

No funding was available for this project.

Declarations of competing interest

The authors declare that they have no known competing financial interests or personal relationships that could have appeared to influence the work reported in this paper.

References

- Adams, T.E., et al., 2000. Structure and function of the type 1 insulin-like growth factor receptor. *Cellular and Molecular Life Sciences CMLS* 57 (7), 1050–1093.
- Anastasiadis, T., et al., 2013. A highly selective dual insulin receptor (IR)/insulin-like growth factor 1 receptor (IGF-1R) inhibitor derived from an extracellular signal-regulated kinase (ERK) inhibitor. *J. Biol. Chem.* 288 (39), 28068–28077.
- Baserga, R., 1995. The insulin-like growth factor 1 receptor: a key to tumor growth? *Cancer Res.* 55 (2), 249–252.
- Belfiore, A., et al., 2009. Insulin receptor isoforms and insulin receptor/insulin-like growth factor receptor hybrids in physiology and disease. *Endocr. Rev.* 30 (6), 586–623.
- Benvenuti, S., et al., 2007. Oncogenic activation of the RAS/RAF signaling pathway impairs the response of metastatic colorectal cancers to anti-epidermal growth factor receptor antibody therapies. *Cancer Res.* 67 (6), 2643–2648.
- Buchanan, J.L., et al., 2011. Discovery of 2, 4-bis-arylamino-1, 3-pyrimidines as insulin-like growth factor-1 receptor (IGF-1R) inhibitors. *Bioorg. Med. Chem. Lett* 21 (8), 2394–2399.
- Buck, E., et al., 2010. Compensatory insulin receptor (IR) activation on inhibition of insulin-like growth factor-1 receptor (IGF-1R): rationale for cotargeting IGF-1R and IR in cancer. *Mol. Cancer Therapeut.* 9 (10), 2652–2664.
- Cao, J., Yee, D., 2021. Disrupting insulin and IGF receptor function in cancer. *Int. J. Mol. Sci.* 22 (2), 555.
- Carboni, J.M., et al., 2009. BMS-754807, a small molecule inhibitor of insulin-like growth factor-1R/IR. *Mol. Cancer Therapeut.* 8 (12), 3341–3349.
- Catalano, R., et al., 2021. The cytoskeleton actin binding protein filamin A impairs both IGF2 mitogenic effects and the efficacy of IGF1R inhibitors in adrenocortical cancer cells. *Cancer Lett.* 497, 77–88.
- Chamberlain, S.D., et al., 2009a. Discovery of 4, 6-bis-anilino-1H-pyrrolo [2, 3-d] pyrimidines: potent inhibitors of the IGF-1R receptor tyrosine kinase. *Bioorg. Med. Chem. Lett* 19 (2), 469–473.
- Chamberlain, S.D., et al., 2009b. Optimization of a series of 4, 6-bis-anilino-1H-pyrrolo [2, 3-d] pyrimidine inhibitors of IGF-1R: elimination of an acid-mediated decomposition pathway. *Bioorg. Med. Chem. Lett* 19 (2), 373–377.
- Chicco, D., 2017. Ten quick tips for machine learning in computational biology. *BioData Min.* 10 (1), 35.
- Christofori, G., Naik, P., Hanahan, D., 1994. A second signal supplied by insulin-like growth factor II in oncogene-induced tumorigenesis. *Nature* 369 (6479), 414–418.
- Christopoulos, P.F., Msaouel, P., Koutsilieris, M., 2015. The role of the insulin-like growth factor-1 system in breast cancer. *Mol. Cancer* 14 (1), 1.
- de Billy, E., et al., 2020. IMM-13. Dual IGF1R/IR inhibitor in combination with GD2-CAR T-Cells as a potent therapeutic strategy for H3K27M-mutant diffuse midline gliomas. *Neuro Oncol.* 22 (Suppl. ment.3) iii362-iii362.
- De Meys, P., Whittaker, J., 2002. Structural biology of insulin and IGF1 receptors: implications for drug design. *Nat. Rev. Drug Discov.* 1 (10), 769–783.
- Denley, A., et al., 2003. The insulin receptor isoform exon 11-IR-A in cancer and other diseases: a review. *Horm. Metab. Res.* 35 (11/12), 778–785.
- Denley, A., et al., 2004. Structural determinants for high-affinity binding of insulin-like growth factor II to insulin receptor (IR)-A, the exon 11 minus isoform of the IR. *Mol. Endocrinol.* 18 (10), 2502–2512.
- Ducray, R., et al., 2011. Discovery of novel imidazo [1, 2-a] pyridines as inhibitors of the insulin-like growth factor-1 receptor tyrosine kinase. *Bioorg. Med. Chem. Lett* 21 (16), 4698–4701.
- Durán, A.n., Martínez, G.C., Pastor, M., 2008. Development and validation of AMANDA, a new algorithm for selecting highly relevant regions in molecular interaction fields. *J. Chem. Inf. Model.* 48 (9), 1813–1823.
- Emmitte, K.A., et al., 2009. Discovery and optimization of imidazo [1, 2-a] pyridine inhibitors of insulin-like growth factor-1 receptor (IGF-1R). *Bioorg. Med. Chem. Lett* 19 (3), 1004–1008.
- Ferguson, D.M., Raber, D.J., 1989. A new approach to probing conformational space with molecular mechanics: random incremental pulse search. *J. Am. Chem. Soc.* 111 (12), 4371–4378.
- Fernandez, M.C., et al., 2019. Inhibition of IGF1R by IGF1R/IR Inhibitor OSI906 as a Targeted Therapy for Glioblastoma: in Vitro & in Vivo Studies, vol. 92. European Society for Paediatric Endocrinology Abstracts.
- Finlay, M.R.V., et al., 2014. Discovery of a potent and selective EGFR inhibitor (AZD9291) of both sensitizing and T790M resistance mutations that spares the wild type form of the receptor. *J. Med. Chem.* 57 (20), 8249–8267.
- Gasteiger, J., Rudolph, C., Sadowski, J., 1990. Automatic generation of 3D-atomic coordinates for organic molecules. *Tetrahedron Comput. Methodol.* 3 (6), 537–547.
- Gill, P.E., Murray, W., Wright, M.H., 1981. *Practical Optimization*.
- Groom, C.R., et al., 2016. The Cambridge structural database. *Acta Crystallogr. B: Structural Science, Crystal Engineering and Materials* 72 (2), 171–179.
- Hempel, C., et al., 2017. Discovery of novel dual inhibitors of receptor tyrosine kinases EGFR and IGF-1R. *J. Enzym. Inhib. Med. Chem.* 32 (1), 271–276.
- Huang, F., et al., 2015. IRS2 copy number gain, KRAS and BRAF mutation status as predictive biomarkers for response to the IGF-1R/IR inhibitor BMS-754807 in colorectal cancer cell lines. *Mol. Cancer Therapeut.* 14 (2), 620–630.
- Ji, Q.-s., et al., 2007. A novel, potent, and selective insulin-like growth factor-I receptor kinase inhibitor blocks insulin-like growth factor-I receptor signaling in vitro and inhibits insulin-like growth factor-I receptor-dependent tumor growth in vivo. *Mol. Cancer Therapeut.* 6 (8), 2158–2167.
- Jin, M., et al., 2010. Discovery of an orally efficacious imidazo [5, 1-f][1, 2, 4] triazine dual inhibitor of IGF-1R and IR. *ACS Med. Chem. Lett.* 1 (9), 510–515.
- Kaplan, S.A., 1984. Cell receptors. *Am. J. Dis. Child.* 138 (12), 1140–1146.
- Kurup, A., Garg, R., Hansch, C., 2001. Comparative QSAR study of tyrosine kinase inhibitors. *Chem. Rev.* 101 (8), 2573–2600.
- Labute, P., Santavy, M., 2007. Locating binding sites in protein structures. *J. Chem. Computing Group*.
- Li, W., et al., 2004. Inhibition of insulin-like growth factor I receptor autophosphorylation by novel 6-5 ring-fused compounds. *Biochem. Pharmacol.* 68 (1), 145–154.
- Li, R., Pourpak, A., Morris, S.W., 2009. Inhibition of the insulin-like growth factor-1 receptor (IGF1R) tyrosine kinase as a novel cancer therapy approach. *J. Med. Chem.* 52 (16), 4981–5004.
- Li, Y.-S., Zhou, L., Ma, X., 2012. Molecular docking and 3D QSAR studies of substituted 4-amino-1H-pyrazolo [3, 4-d] pyrimidines as insulin-like growth factor-1 receptor (IGF1R) inhibitors. *Med. Chem. Res.* 21 (10), 3301–3311.
- Liu, Y., Gray, N.S., 2006a. Rational design of inhibitors that bind to inactive kinase conformations. *Nat. Chem. Biol.* 2 (7), 358–364.
- Liu, Y., Gray, N.S., 2006b. Rational design of inhibitors that bind to inactive kinase conformations. *Nat. Chem. Biol.* 2 (7), 358.
- Liu, X., et al., 2010. Discovery and SAR of thiazolidine-2, 4-dione analogues as insulin-like growth factor-1 receptor (IGF-1R) inhibitors via hierarchical virtual screening. *J. Med. Chem.* 53 (6), 2661–2665.
- Luo, R.Z.-T., et al., 1999. Quaternary structure of the insulin-insulin receptor complex. *Science* 285 (5430), 1077–1080.
- Marsilje, T.H., et al., 2013. Synthesis, structure–activity relationships, and in vivo efficacy of the novel potent and selective anaplastic lymphoma kinase (ALK) inhibitor 5-Chloro-N 2-(2-isopropoxy-5-methyl-4-(piperidin-4-yl) phenyl)-N 4-(2-(isopropylsulfonyl) phenyl) pyrimidine-2, 4-diamine (LDK378) currently in phase 1 and phase 2 clinical trials. *J. Med. Chem.* 56 (14), 5675–5690.
- Mayer, S.C., et al., 2008. Lead identification to generate isoquinolinedione inhibitors of insulin-like growth factor receptor (IGF-1R) for potential use in cancer treatment. *Bioorg. Med. Chem. Lett* 18 (12), 3641–3645.
- Miller, L.M., et al., 2009. Lead identification to generate 3-cyanoquinoline inhibitors of insulin-like growth factor receptor (IGF-1R) for potential use in cancer treatment. *Bioorg. Med. Chem. Lett* 19 (1), 62–66.
- Mosthaf, L., et al., 1990. Functionally distinct insulin receptors generated by tissue-specific alternative splicing. *EMBO J.* 9 (8), 2409.
- Muddassar, M., et al., 2008. Receptor guided 3D-QSAR: a useful approach for designing of IGF-1R inhibitors. *BioMed Res. Int.* 2008.
- Mulvihill, M.J., et al., 2008. Novel 2-phenylquinolin-7-yl-derived imidazo [1, 5-a] pyrazines as potent insulin-like growth factor-I receptor (IGF-1R) inhibitors. *Bioorg. Med. Chem.* 16 (3), 1359–1375.
- Mulvihill, M.J., et al., 2009. Discovery of OSI-906: a selective and orally efficacious dual inhibitor of the IGF-1 receptor and insulin receptor. *Future Med. Chem.* 1 (6), 1153–1171.
- Munawar, S., et al., 2018. Experimentally validated pharmacoinformatics approach to predict hERG inhibition potential of new chemical entities. *Front. Pharmacol.* 9, 1035.
- Nemecek, C., et al., 2010. Design of potent IGF-1R inhibitors related to bis-azaindoles. *Chem. Biol. Drug Des.* 76 (2), 100–106.
- Ottensmeyer, F., et al., 2000. Mechanism of transmembrane signaling: insulin binding and the insulin receptor. *Biochemistry* 39 (40), 12103–12112.
- Papa, V., Belfiore, A., 1996. Insulin receptors in breast cancer: biological and clinical role. *J. Endocrinol. Investig.* 19 (5), 324–333.
- Párrizas, M., et al., 1997. Specific inhibition of insulin-like growth factor-1 and insulin receptor tyrosine kinase activity and biological function by tyrphostins. *Endocrinology* 138 (4), 1427–1433.
- Pashaa, M.K., Munawara, K., Qureshi, A.T., 2021. Application of the docking protocol optimization for inhibitors of IGF-1R and IR and understanding them through artificial intelligence and bibliography. *I. J. Educ. Manag. Eng.* 4, 1–11.
- Pastor, M., et al., 2000. GRIND-INdependent descriptors (GRIND): a novel class of alignment-independent three-dimensional molecular descriptors. *J. Med. Chem.* 43 (17), 3233–3243.
- Ramdhare, A.S., Nandave, M., 2016. Rediscovery of IGF-1R targeted inhibitors from an approved drugs database through receptor-based pharmacophore modeling and docking. *Indo Am. J. Pharm. Res.* 6 (1), 4295–4301.
- Rosen, O.M., et al., 1983. Phosphorylation activates the insulin receptor tyrosine protein kinase. *Proceedings of the National Academy of Sciences* 80 (11), 3237–3240.
- Sabari, J.K., et al., 2017. The activity, safety, and evolving role of brigatinib in patients with ALK-rearranged non-small cell lung cancers. *OncoTargets Ther.* 10, 1983.
- Sadowski, J., Gasteiger, J., Klebe, G., 1994. Comparison of automatic three-dimensional model builders using 639 X-ray structures. *J. Chem. Inf. Comput. Sci.* 34 (4), 1000–1008.
- Sciacca, L., et al., 2002. IGF-I receptor-deficient leiomyosarcoma cells autocrine IGF-II induces cell invasion and protection from apoptosis via the insulin receptor isoform A. *Oncogene* 21 (54), 8240–8250.
- Sheridan, R.P., et al., 2009. QSAR models for predicting the similarity in binding profiles for pairs of protein kinases and the variation of models between experimental data sets. *J. Chem. Inf. Model.* 49 (8), 1974–1985.
- Sperandio, O., Petitjean, M., Tufféry, P., 2009. wwLigCSRR: a 3D ligand-based server for hit identification and optimization. *Nucleic Acids Res.* 37 (Suppl. 2), W504–W509.

- Stauffer, F., et al., 2016. Identification of a 5-[3-phenyl-(2-cyclic-ether)-methylether]-4-aminopyrrolo [2, 3-d] pyrimidine series of IGF-1R inhibitors. *Bioorg. Med. Chem. Lett* 26 (8), 2065–2067.
- Su, M., et al., 2020. Structural basis of the activation of heterotrimeric Gs-protein by isoproterenol-bound β 1-adrenergic receptor. *Mol. Cell* 80 (1), 59–71.e4.
- Sushko, I., et al., 2011. Online chemical modeling environment (OCHEM): web platform for data storage, model development and publishing of chemical information. *J. Comput. Aided Mol. Des.* 25 (6), 533–554.
- Taha, M.O., et al., 2007. Discovery of new potent human protein tyrosine phosphatase inhibitors via pharmacophore and QSAR analysis followed by in silico screening. *J. Mol. Graph. Model.* 25 (6), 870–884.
- Thinn, A.M.M., et al., 2018. Autonomous conformational regulation of β 3 integrin and the conformation-dependent property of HPA-1a alloantibodies. *Proc. Natl. Acad. Sci. U.S.A.* 115 (39), E9105–E9114.
- Umehara, H., et al., 2018. Preclinical and phase I clinical studies of KW-2450, a dual IGF-1R/IR tyrosine kinase inhibitor, in combination with lapatinib and letrozole. *Therapeutic Adv. Med. Oncol* 10, 1758835918786858.
- Wang, R., Gao, Y., Lai, L., 2000. LigBuilder: a multi-purpose program for structure-based drug design. *Molecular modeling annual* 6 (7–8), 498–516.
- Wang, A., et al., 2017. Discovery of (R)-1-(3-(4-Amino-3-(3-chloro-4-(pyridin-2-ylmethoxy) phenyl)-1 H-pyrazolo [3, 4-d] pyrimidin-1-yl) piperidin-1-yl) prop-2-en-1-one (CHMFL-EGFR-202) as a novel irreversible EGFR mutant kinase inhibitor with a distinct binding mode. *J. Med. Chem.* 60 (7), 2944–2962.
- Wishart, D., et al., *DrugBank: A Comprehensive Resource for in Silico Drug Discovery and Explorat.*
- Wood, E.R., et al., 2009. Discovery of an inhibitor of insulin-like growth factor 1 receptor activation: implications for cellular potency and selectivity over insulin receptor. *Biochem. Pharmacol.* 78 (12), 1438–1447.
- Wu, W., et al., 2017. Co-targeting IGF-1R and autophagy enhances the effects of cell growth suppression and apoptosis induced by the IGF-1R inhibitor NVP-AEW541 in triple-negative breast cancer cells. *PLoS One* 12 (1), e0169229.
- Yu, H., Rohan, T., 2000. Role of the insulin-like growth factor family in cancer development and progression. *J. Natl. Cancer Inst.* 92 (18), 1472–1489.
- Zwick, E., Bange, J., Ullrich, A., 2002. Receptor tyrosine kinases as targets for anticancer drugs. *Trends Mol. Med.* 8 (1), 17–23.